

Neutrino elastic scattering on polarized electrons as a tool for probing the neutrino nature

A. Błaut^{a,1}, W. Sobków^{b,1}

¹ Institute of Theoretical Physics, University of Wrocław, Pl. M. Born 9, PL-50-204 Wrocław, Poland

Received: date / Accepted: date

Abstract Possibility of using the polarized electron target (PET) for testing the neutrino nature is considered. It is assumed that the incoming ν_e beam is the superposition of left chiral (LC) states with right chiral (RC) ones. Consequently the non-vanishing transversal components of ν_e spin polarization may appear, both T-even and T-odd. ν_e s are produced by the low energy monochromatic (un)polarized emitter located at a near distance from the hypothetical detector which is able to measure both the azimuthal angle and the polar angle of the recoil electrons, and/or also the energy of the outgoing electrons with a high resolution. A detection process is the elastic scattering of ν_e s (Dirac or Majorana) on the polarized electrons. LC ν_e s interact mainly by the standard $V - A$ interaction, while RC ones participate only in the non-standard $V + A$, scalar S_R , pseudoscalar P_R and tensor T_R interactions. All the interactions are of flavour-conserving type (FC). We show that a distinction between the Dirac and the Majorana ν_e s is possible both for the longitudinal and the transversal ν_e polarizations.

In the first case a departure from the standard prediction of the azimuthal asymmetry of recoil electrons is caused by the interferences between the non-standard complex S and T couplings, proportional to the angular correlations (T-even and T-odd) among the polarization of the electron target, the incoming neutrino momentum and the outgoing electron momentum. It is shown that such a deviation would indicate the Dirac ν_e nature and the presence of time reversal symmetry violation (TRSV) interactions. It is remarkable that the result is conclusive for all Majorana non-standard couplings.

In the second case the azimuthal asymmetries, polar distribution and energy spectrum of scattered electrons are sensitive to the interference terms between the standard and ex-

otic interactions, proportional to the various angular correlations among the transversal ν_e spin polarization, the electron target polarization, the incoming ν_e momentum and the outgoing electron momentum. In the particular case of the $V - A$ and S couplings the precise measurement of some observables, e.g. the spectrum, can distinguish between the Dirac and the Majorana ν_e s as long as the incoming ν_e beam has non-vanishing transversal polarization. Our model-independent study is carried out for the flavour ν_e eigenstates in the relativistic ν_e limit.

1 Introduction

One of the basic questions in neutrino physics is whether the ν s are Dirac or Majorana fermions. At present, the neutrinoless double beta decay is viewed as the main tool to investigate ν s nature [1–3], however the purely leptonic processes (e.g. the neutrino-electron elastic scattering (NEES)) may also shed some light on this problem [4, 5]. Kayser and Langacker have analyzed the ν s nature problem in the context of non-zero ν s mass and of the standard model (SM) $V - A$ interaction [6–10] of only the LC ν s. There is an alternative opportunity of distinguishing between Majorana and Dirac ν s by admitting the exotic $V + A$, scalar S , pseudoscalar P and tensor T interactions coupling to the LC and RC ν s in the leptonic processes within the relativistic ν limit. The appropriate tests have been considered by Rosen [11] and Dass [12] (see also [13–24] for other works devoted to the ν nature and the non-standard ν properties). The above ideas involve the unpolarized detection target. When the target-electrons are polarized by an external magnetic field, one has a possibility of changing the rate of weak interaction by inverting the direction of magnetic field. This feature is very important in the detection of low energy ν_e s because the background level would be precisely controlled [25]. PET

^ae-mail: arkadiusz.blaut@uwr.edu.pl

^be-mail: wieslaw.sobkow@uwr.edu.pl (corresponding author)

seems to be a more sensitive laboratory for probing the ν nature and TRSV in the leptonic processes than the unpolarized target due to the mentioned control of contribution of the interaction to the cross section. It is worth reminding that the PET has been proposed to test the flavour composition of (anti)neutrino beam [26] and various effects of non-standard physics. We mean the neutrino magnetic moments [27, 28], TRSV in the (semi)leptonic processes [29, 30], axions, spin-spin interaction in gravitation [31–34]. The possibility of using polarized targets of nucleons and of electrons for the fermionic, scalar and vector dark matter detection is also worth noticing [35–37]. The methods of producing the spin-polarized gasses such as helium, argon and xenon are described in [38, 39].

It is also essential to mention the measurements confirming the possibility of realizing the polarized target crystal of Gd_2SiO_5 (GSO) doped with Cerium (GSO:Ce) [40].

Let us recall that there is no difference between Dirac and Majorana ν s in the case of NEES with the standard V-A interaction in the relativistic limit, when the target is unpolarized.

The SM does not allow the clarification of the origin of parity violation, observed baryon asymmetry of universe [41] through a single CP-violating phase of the Cabibbo-Kobayashi-Maskawa quark-mixing matrix (CKM) [42] and other fundamental problems. This has led to the appearance of many non-standard models: the left-right symmetric models (LRS) [43–46], composite models [47–49], models with extra dimensions (MED) [50] and the unparticle models (UP) [51–53]. There is a rich literature devoted to the phenomenological aspects of the non-standard interactions of LC and in particular RC ν s: [54–81]. It is also noteworthy that the current experimental results still leave some space for the scenarios with the exotic interactions.

Recently the study of the ν nature with a use of PET in the case of standard V-A interaction, when the evolution of ν spin polarization in the astrophysical environments is admitted, has been carried out in [82, 83].

In this paper we consider the elastic scattering of low energy ν_e s ($\sim 1\text{MeV}$) on the polarized electrons of target in the presence of non-standard complex scalar, pseudoscalar, tensor couplings and $V + A$ interaction as a useful tool for testing the ν nature. We show how the various types of azimuthal asymmetry, the polar distribution and the energy spectrum of scattered electrons enable the distinguishing between the Dirac and the Majorana ν_e s both for the longitudinal and the transversal ν_e polarizations, taking into account TRSV. Both theoretically possible scenarios of physics beyond SM deal with FC standard and non-standard interactions. Our study is model-independent and carried out for the flavour ν_e eigenstates (Dirac and Majorana) in the relativistic limit. One assumes that the monochromatic low energy and (un)polarized ν_e emitter with a high activity is

placed at a near distance from the detector (or at the detector centre). The hypothetical detector is assumed to be able to measure both the azimuthal angle ϕ_e and the polar angle θ_e of the recoil electrons, and/or also the energy of the outgoing electrons with a high resolution, Fig.1. We utilize the experimental values of standard couplings: $c_V^L = 1 - 0.04$, $c_A^L = 1 - 0.507$ to evaluate the predicted effects [84], where the indexes V, A and L denote the vector, the axial interactions and the left-handed chirality of ν_e s, respectively. We assume the values of exotic couplings which are compatible with the constraints on non-standard interactions obtained in our previous paper [85] and by various authors: [86, 87]. The laboratory differential cross sections (see Appendix 1 for Majorana ν_e s and [30] for the Dirac case) are calculated with the use of the covariant projectors for the incoming ν_e s (including both the longitudinal and the transversal components of the spin polarization) in the relativistic limit and for the polarized target-electrons, respectively [88].

2 Elastic scattering of Dirac electron neutrinos on polarized electrons

We analyze a scenario in which the incoming Dirac ν_e beam is assumed to be the superposition of LC states with RC ones. The detection process is the elastic scattering of Dirac ν_e s on the polarized target-electrons. The relative orientation of the incoming ν_e , the polarized electron target and the outgoing electron is depicted in Fig. 1, where the notation for the relevant quantities is explained.

LC ν_e s interact mainly by the standard $V - A$ interaction and a small admixture of the non-standard scalar S_L , pseudoscalar P_L , tensor T_L interactions, while RC ones take part only in the exotic $V + A$ and S_R, P_R, T_R interactions. As a result of the superposition of the two chiralities the spin polarization vector has the non-vanishing transversal polarization components, which may give rise to both T-even and T-odd effects. As an example of the process in which the transversal ν polarization may be produced, we refer to the ref. [89], where the muon capture by proton has been considered. The amplitude for the $\nu_e e^-$ scattering in low energy region is in the form:

$$\begin{aligned}
 M_{\nu_e e^-}^D = \frac{G_F}{\sqrt{2}} \{ & (\bar{u}_{e'} \gamma^\alpha (c_V^L - c_A^L \gamma_5) u_e) (\bar{u}_{\nu_e'} \gamma_\alpha (1 - \gamma_5) u_{\nu_e}) \\
 & + (\bar{u}_{e'} \gamma^\alpha (c_V^R + c_A^R \gamma_5) u_e) (\bar{u}_{\nu_e'} \gamma_\alpha (1 + \gamma_5) u_{\nu_e}) \quad (1) \\
 & + c_S^R (\bar{u}_{e'} u_e) (\bar{u}_{\nu_e'} (1 + \gamma_5) u_{\nu_e}) \\
 & + c_P^R (\bar{u}_{e'} \gamma_5 u_e) (\bar{u}_{\nu_e'} \gamma_5 (1 + \gamma_5) u_{\nu_e}) \\
 & + \frac{1}{2} c_T^R (\bar{u}_{e'} \sigma^{\alpha\beta} u_e) (\bar{u}_{\nu_e'} \sigma_{\alpha\beta} (1 + \gamma_5) u_{\nu_e}) \\
 & + c_S^L (\bar{u}_{e'} u_e) (\bar{u}_{\nu_e'} (1 - \gamma_5) u_{\nu_e}) \\
 & + c_P^L (\bar{u}_{e'} \gamma_5 u_e) (\bar{u}_{\nu_e'} \gamma_5 (1 - \gamma_5) u_{\nu_e}) \}
 \end{aligned}$$

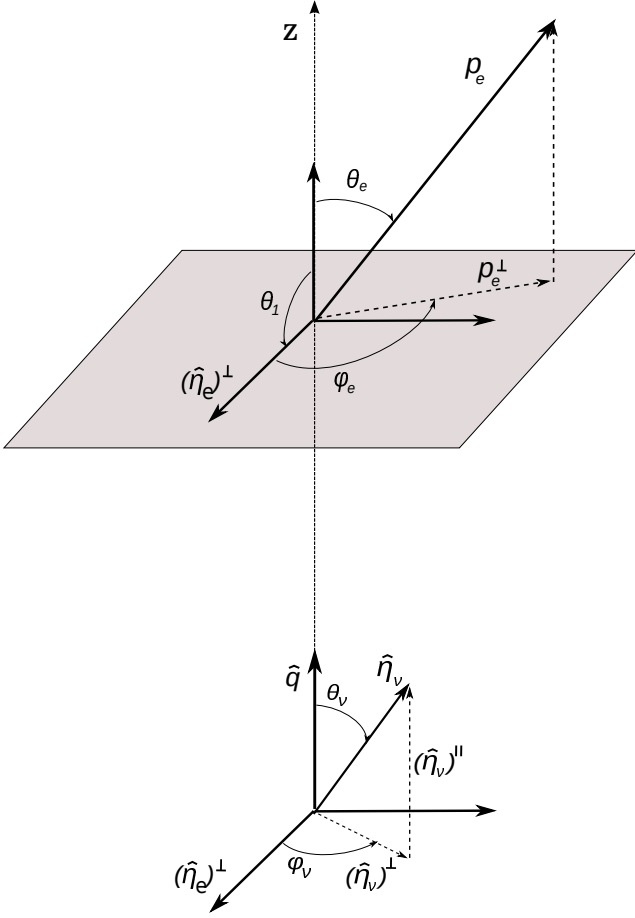


Fig. 1 The reaction plane is spanned by the ν_e LAB momentum unit vector $\hat{\mathbf{q}}$ and the electron polarization vector of the target $\hat{\mathbf{h}}_e$. θ_1 is the angle between $\hat{\mathbf{h}}_e$ and $\hat{\mathbf{q}}$ (on the plot $\theta_1 = \pi/2$ so in this case $\hat{\mathbf{h}}_e = (\hat{\mathbf{h}}_e)^\perp$). θ_e is the polar angle between $\hat{\mathbf{q}}$ and the unit vector $\hat{\mathbf{p}}_e$ of the recoil electron momentum. ϕ_e is the angle between $(\hat{\mathbf{h}}_e)^\perp$ and the transversal component of outgoing electron momentum $(\hat{\mathbf{p}}_e)^\perp$. ϕ_ν and θ_ν are the azimuthal and the polar angles of the unit polarization vector of the incoming neutrino, $\hat{\mathbf{h}}_\nu = (\sin \theta_\nu \cos \phi_\nu, \sin \theta_\nu \sin \phi_\nu, \cos \theta_\nu)$.

$$+ \frac{1}{2} c_T^L (\bar{u}_{e'} \sigma^{\alpha\beta} u_e) (\bar{u}_{\nu_e} \sigma_{\alpha\beta} (1 - \gamma_5) u_{\nu_e}) \},$$

where $G_F = 1.1663788(7) \times 10^{-5} \text{ GeV}^{-2} (0.6 \text{ ppm})$ [90] is the Fermi constant. The coupling constants are denoted as $c_V^{L,R}, c_A^{L,R}, c_S^{R,L}, c_P^{R,L}, c_T^{R,L}$ respectively to the incoming ν_e of left- and right-handed chirality. All the non-standard couplings $c_S^{R,L}, c_P^{R,L}, c_T^{R,L}$ are the complex numbers denoted as $c_S^R = |c_S^R| e^{i\theta_{S,R}}, c_S^L = |c_S^L| e^{i\theta_{S,L}}$, etc. Reality of $c_V^{L,R}, c_A^{L,R}$ coupling constants follows from the hermiticity of the interaction lagrangian; for the same reason we take into account the relations between the non-standard complex couplings with left- and right-handed chirality, $c_{S,T,P}^L = c_{S,T,P}^{*R}$. All results are stated in terms of R couplings.

3 Elastic scattering of Majorana electron neutrinos on polarized electrons

The fundamental difference between Majorana and Dirac ν_e s arises from a fact that Majorana ν_e s do not participate in the vector V and tensor T interactions. This is a direct consequence of the (u, v) -mode decomposition of the Majorana field. The amplitude for NEES on PET for Majorana low energy ν_e s is as follows:

$$M_{\nu_e e^-}^M = \frac{2G_F}{\sqrt{2}} \{ -(\bar{u}_{e'} \gamma^\alpha (c_V - c_A \gamma_5) u_e) (\bar{u}_{\nu_e} \gamma_\alpha \gamma_5 u_{\nu_e}) \quad (2) \\ + (\bar{u}_{e'} u_e) [c_S^L (\bar{u}_{\nu_e} (1 - \gamma_5) u_{\nu_e}) + c_S^R (\bar{u}_{\nu_e} (1 + \gamma_5) u_{\nu_e})] \\ + (\bar{u}_{e'} \gamma_5 u_e) [-c_P^L (\bar{u}_{\nu_e} (1 - \gamma_5) u_{\nu_e}) + c_P^R (\bar{u}_{\nu_e} (1 + \gamma_5) u_{\nu_e})] \}.$$

We see that the ν_e contributions from A, S, P are multiplied by the factor of 2 as a result of the Majorana condition. The indexes $L, (R)$ for the standard interactions are omitted. It means that both LC and RC ν_e s may take part in the above interactions. All the other assumptions are the same as for the Dirac case.

4 Distinguishing between Dirac and Majorana neutrinos through azimuthal asymmetries of recoil electrons

In this section we analyze the possibility of distinguishing the Dirac from the Majorana ν_e s through probing the azimuthal asymmetries, A, A_y, A_{θ_e} , of recoil electrons. The asymmetry functions are defined by the following formulas:

$$A(\Phi) := \frac{\int_{\Phi}^{\Phi+\pi} \frac{d\sigma}{d\phi_e} d\phi_e - \int_{\Phi+\pi}^{\Phi+2\pi} \frac{d\sigma}{d\phi_e} d\phi_e}{\int_{\Phi}^{\Phi+\pi} \frac{d\sigma}{d\phi_e} d\phi_e + \int_{\Phi+\pi}^{\Phi+2\pi} \frac{d\sigma}{d\phi_e} d\phi_e}, \quad (3)$$

$$A_y(\Phi) := \frac{\int_{\Phi}^{\Phi+\pi} \frac{d^2\sigma}{d\phi_e dy} d\phi_e - \int_{\Phi+\pi}^{\Phi+2\pi} \frac{d^2\sigma}{d\phi_e dy} d\phi_e}{\int_{\Phi}^{\Phi+\pi} \frac{d^2\sigma}{d\phi_e dy} d\phi_e + \int_{\Phi+\pi}^{\Phi+2\pi} \frac{d^2\sigma}{d\phi_e dy} d\phi_e}, \quad (4)$$

$$A_{\theta_e}(\Phi) := \frac{\int_{\Phi}^{\Phi+\pi} \frac{d^2\sigma}{d\phi_e d\theta_e} d\phi_e - \int_{\Phi+\pi}^{\Phi+2\pi} \frac{d^2\sigma}{d\phi_e d\theta_e} d\phi_e}{\int_{\Phi}^{\Phi+\pi} \frac{d^2\sigma}{d\phi_e d\theta_e} d\phi_e + \int_{\Phi+\pi}^{\Phi+2\pi} \frac{d^2\sigma}{d\phi_e d\theta_e} d\phi_e}. \quad (5)$$

These observables are functions of the asymmetry angle Φ (the interpretation of Φ follows from the definitions of eqs. (3-5) and Fig. 1: Φ is measured with respect to the transverse electron polarization vector of target $(\hat{\mathbf{h}}_e)^\perp$); by Φ_{max} we denote the location of their maxima. In what follows we shall use the normalized, dimensionless kinetic energy of the recoil electrons y , defined by

$$y \equiv \frac{T_e}{E_\nu} = \frac{m_e}{E_\nu} \frac{2 \cos^2(\theta_e)}{(1 + \frac{m_e}{E_\nu})^2 - \cos^2(\theta_e)}, \quad (6)$$

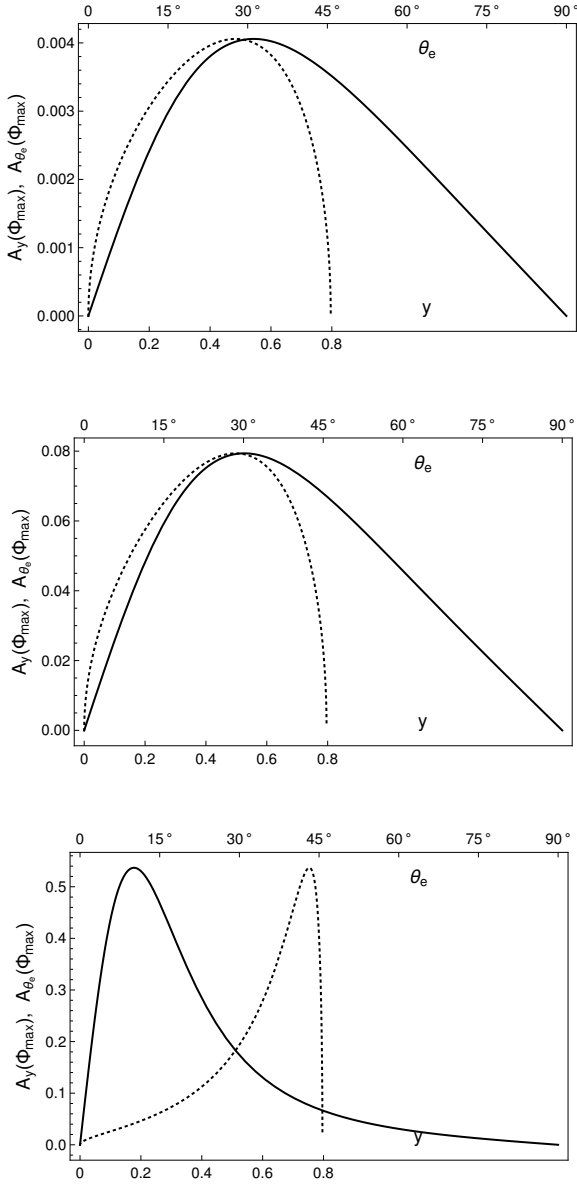


Fig. 2 Dirac (or Majorana) ν_e with $V-A$ interaction: plot of $A_y(\Phi_{max})$ as a function y (dotted line) and $A_{\theta_e}(\Phi_{max})$ as a function of θ_e (solid line) for $\hat{\eta}_\nu \cdot \hat{\mathbf{q}} = -1$, $E_\nu = 1 \text{ MeV}$, $\Phi_{max} = \pi/2$; upper plot for $\theta_1 = 0.1$; middle plot for $\theta_1 = \pi/2$; lower plot for $\theta_1 = \pi - 0.1$.

where T_e is the kinetic energy of the recoil electron, E_ν is the incoming ν_e energy, m_e is the electron mass. Fig. 2 shows the asymmetries $A_y(\Phi_{max})$, $A_{\theta_e}(\Phi_{max})$ for the standard $V-A$ interaction with $\hat{\eta}_\nu \cdot \hat{\mathbf{q}} = -1$. Although the orientation of the asymmetry axis is fixed at $\Phi_{max} = \pi/2$ the magnitude of the asymmetries may change with y and θ_e . We see that the maximum values of $A_y(\Phi_{max})$ and $A_{\theta_e}(\Phi_{max})$ also depend on the angle θ_1 between $\hat{\eta}_e$ and $\hat{\mathbf{q}}$: they grow from 0.004 for $\theta_1 = 0.1$ (upper plot) to 0.54 for $\theta_1 = \pi - 0.1$ (lower plot). However all curves on the diagrams are identical for the Dirac and the Majorana ν_e s therefore the asymmetries

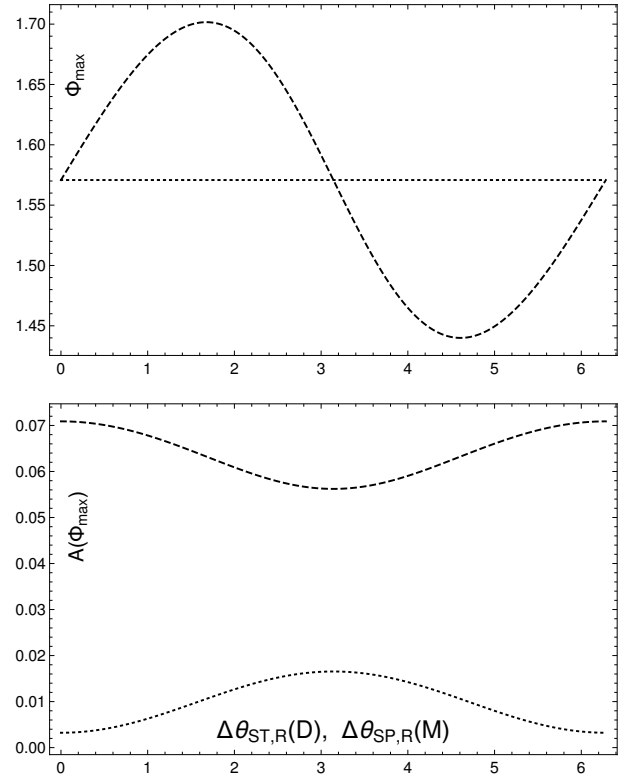


Fig. 3 Upper plot (dashed line) is the dependence of Φ_{max} on $\Delta\theta_{ST,R}(D)$ for Dirac ν_e in case of $V-A$, S_R and T_R interactions when $|c_S^R| = |c_T^R| = 0.2$. Upper plot (dotted line) is the dependence of Φ_{max} on $\Delta\theta_{SP,R}(M)$ for Majorana ν_e in case of $V-A$, S_R and P_R couplings when $|c_S^R| = |c_P^R| = 0.2$. Both scenarios assume $\hat{\eta}_\nu \cdot \hat{\mathbf{q}} = -1$, $\theta_1 = \pi/2$, $E_\nu = 1 \text{ MeV}$. Lower plot is the dependence of $A(\Phi_{max})$ on $\Delta\theta_{ST,R}(D)$ for Dirac ν_e (dashed line) and on $\Delta\theta_{SP,R}(M)$ for Majorana ν_e (dotted line), respectively, with same assumptions as for Φ_{max} .

can not discriminate between the two ν types even if the target-electrons are polarized.

The presence of non-standard S, T, P complex couplings of Dirac ν_e s with $\hat{\eta}_\nu \cdot \hat{\mathbf{q}} = -1$ leads to the non-vanishing triple angular correlations composed of $\hat{\mathbf{q}}, \hat{\mathbf{p}}_e, (\hat{\eta}_e)^\perp$ vectors. These terms not only play a role in distinguishing between the Dirac and the Majorana ν_e s but in the Dirac case they allow to search for the effects of TRSV in NEES. Fig. 3 shows how the asymmetry axis location Φ_{max} (upper plot) and the magnitude of $A(\Phi_{max})$ (lower plot) depend on the phase differences $\Delta\theta_{ST,R}(D) = \theta_{S,R} - \theta_{T,R}$ for the Dirac ν_e s (dashed lines) and $\Delta\theta_{SP,R}(M) = \theta_{S,R} - \theta_{P,R}(M)$ for the Majorana ν_e s (dotted lines) when $\theta_1 = \pi/2$. To explain the origin of the difference we give the formulas for $A(\Phi)$ with assumed values of $\theta_1 = \pi/2$, $\theta_\nu = \pi$, the experimental standard couplings and $E_\nu = 1 \text{ MeV}$. For the Dirac scenario with $V-A$, S_R and T_R interactions, it reads:

$$A_D^{(S,R)(T,R)}(\Phi) = - \left\{ \left[3.354(-\sin(\Phi))(8|c_S^R||c_T^R|\cos(\Delta\theta_{ST,R}) + 8|c_T^R|^2 + 1.369) - 10|c_S^R||c_T^R|\sin(\Delta\theta_{ST,R})\cos(\Phi) \right] \right\} \quad (7)$$

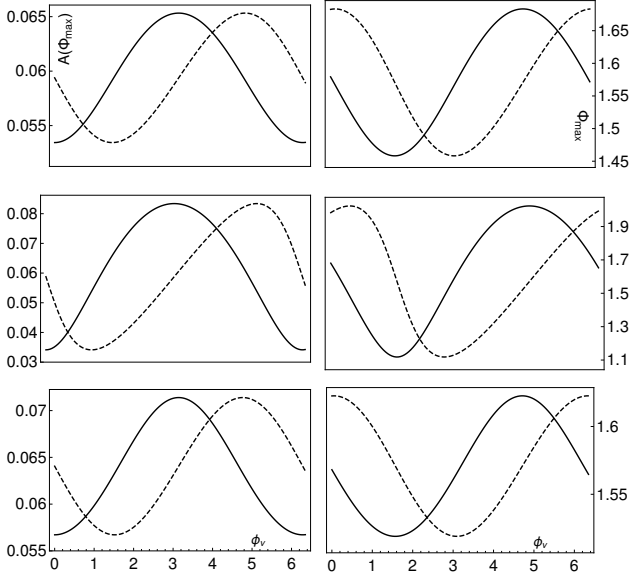


Fig. 4 Superposition of LC ν_e s with RC ones in presence of non-standard couplings with $\hat{\eta}_V \cdot \hat{\mathbf{q}} = -0.95$: dependence of $A(\Phi_{max})$ on ϕ_V (solid line) and Φ_{max} on ϕ_V (dashed line) for $E_V = 1 \text{ MeV}$, $\theta_1 = \pi/2$. TRSC: upper left plot for Dirac case of $V-A$ and S_R when $|c_S^R| = 0.2$, $\theta_{S,R} = 0$; middle left plot for Majorana case of $V-A$ with S_R when $|c_S^R| = 0.2$, $\theta_{S,R} = 0$; lower left plot for Dirac case of $V-A$ with T_R when $|c_T^R| = 0.2$, $\theta_{T,R} = 0$. TRSV: upper right plot for Dirac scenario with $V-A$ and S_R when $|c_S^R| = 0.2$, $\theta_{S,R} = \pi/2$; middle right plot for Majorana case of $V-A$ with S_R when $|c_S^R| = 0.2$, $\theta_{S,R} = \pi/2$; lower right plot for Dirac case of $V-A$ and T_R when $|c_T^R| = 0.2$, $\theta_{T,R} = \pi/2$.

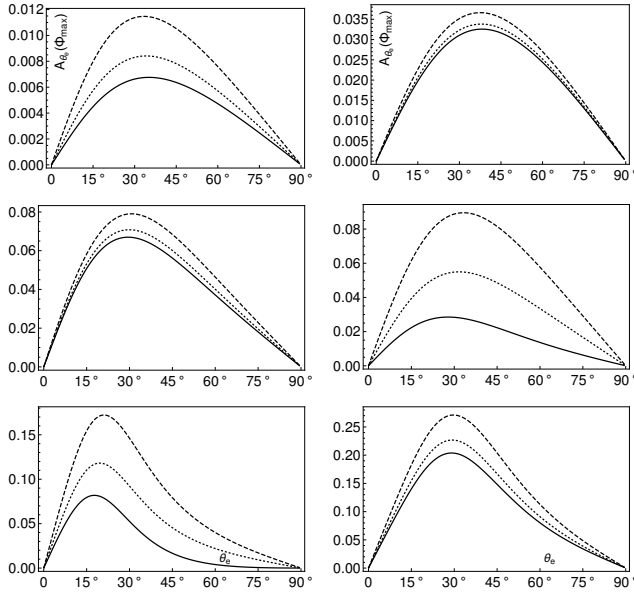


Fig. 5 Superposition of LC ν_e s with RC ones in presence of non-standard couplings with $\hat{\eta}_V \cdot \hat{\mathbf{q}} = -0.95$: plot of $A_{\theta_e}(\Phi_{max})$ as a function of θ_e for the case of $V-A$ with S_R when $E_V = 1 \text{ MeV}$, $\phi_V = 0$; left column for Dirac ν_e , right column for Majorana ν_e ; upper plot for $\theta_1 = 0.1$; middle plot for $\theta_1 = \pi/2$; lower plot for $\theta_1 = \pi - 0.1$; solid line for $|c_S^R| = 0.3$, $\theta_{S,R} = 0$; dotted line for $|c_S^R| = 0.3$, $\theta_{S,R} = \pi/4$; dashed line for $|c_S^R| = 0.3$, $\theta_{S,R} = \pi/2$.

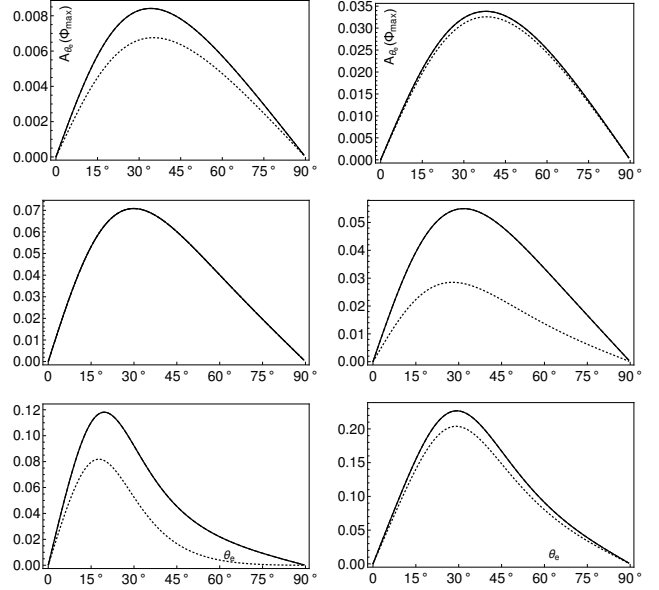


Fig. 6 Superposition of LC ν_e s with RC ones in presence of non-standard couplings with $\hat{\eta}_V \cdot \hat{\mathbf{q}} = -0.95$: plot of $A_{\theta_e}(\Phi_{max})$ as a function of θ_e for the case of $V-A$ with S_R when $E_V = 1 \text{ MeV}$, $\phi_V = \pi/4$; left column for Dirac ν_e , right column for Majorana ν_e ; upper plot for $\theta_1 = 0.1$; middle plot for $\theta_1 = \pi/2$; lower plot for $\theta_1 = \pi - 0.1$; solid line for $|c_S^R| = 0.3$, $\theta_{S,R} = 0$; dotted line for $|c_S^R| = 0.3$, $\theta_{S,R} = \pi/4$; dashed line for $|c_S^R| = 0.3$, $\theta_{S,R} = \pi/2$.

$$-1.369 \sin(\Phi)) \Big] / \left[12(|c_S^R|^2 + 5|c_T^R|^2 + 1.881) + 1.5(|2c_S^R|^2 + 6|c_T^R|^2 + 1.651) + 8(|c_S^R|^2 + 14|c_T^R|^2 + 6.552) - 44|c_S^R||c_T^R|\cos(\Delta\theta_{ST,R}) + 77.462 \right].$$

The corresponding formula for $A(\Phi)$ in the Majorana case with $V-A$, S_R , P_R and $V+A$ couplings is of the form:

$$A_M^{(All)}(\Phi) = - \left\{ 3.354 \sin(\Phi) \left[4|c_P^R||c_S^R|\cos(\Delta\theta_{SP,R}) - 1.369 \right] / \left[16(|c_P^R|^2 + 2.875|c_S^R|^2 + 4.841) \right] \right\}.$$

It can be noticed that these expressions explicitly reveal different dependence on the azimuthal angle Φ in the two cases. Thus, it is not possible to reproduce the dashed curve of Fig. 3, which describes the Dirac ν beam, by using the all possible non-standard (flavour-conserving) Majorana ν interactions.

Another possibilities are related to the $\hat{\eta}_V \cdot \hat{\mathbf{q}} \neq -1$ case. When we assume that the incoming ν_e beam is the superposition of LC ν s with RC ones and there is an experimental control of the angle ϕ_V connected with $(\hat{\eta}_V)^\perp$, we have new opportunities of testing the ν_e nature and TRSV. Fig. 4 illustrates the asymmetry A in this case. It probes the dependence of $A(\Phi_{max})$ (solid line) and the asymmetry axes location Φ_{max} (dashed line) on ϕ_V . The plot compares behavior of the Dirac (S_R , T_R) and the Majorana (S_R) ν s additionally

taking into account TRSC (left column) and TRSV (right column) options. The detection of a non-trivial dependence of the asymmetry on the ϕ_v shown in Fig. 4 would indicate the existence of exotic scalar or tensor couplings of RC vs. The precise measurement of the magnitude of $A(\Phi_{max})$ would help to detect TRSV, however it can be difficult to distinguish between the Dirac and the Majorana ν_e s.

The Figs. (5-6) display the impact of θ_1 and ϕ_v on the possible values of the asymmetry $A_{\theta_e}(\Phi_{max})$ for the scalar interactions. We see that this measurement is sensitive to the presence of exotic couplings, offers the possibility of the distinction between the Dirac and the Majorana ν_e s, and allows the detection of TRSV effects. For the sake of the illustration of the variety of possible outcomes we point on the most noticeable characteristics of the diagrams presented in Fig. 5. The maximum values of $A_{\theta_e}(\Phi_{max})$ for $\theta_1 = 0.1$ increase to 0.012 in the Dirac case (dashed line in left upper plot), and to 0.035 in the Majorana case (dashed line in right upper plot) in comparison to the standard expectation of 0.004, shown in Fig 2. When $\theta_1 = \pi/2$ the magnitude of $A_{\theta_e}(\Phi_{max})$ may decrease to around 0.02 for the Majorana ν_e s (solid line in middle right plot), while the standard prediction gives 0.08 at $\theta_e = \pi/6$. The maximum value of $A_{\theta_e}(\Phi_{max})$ for $\theta_1 = \pi - 0.1$ decreases to $0.08 - 0.17$ for the Dirac ν_e s (lower left plot) and to $0.2 - 0.27$ in the Majorana case (lower right plot), compared to the standard expectation of 0.54. In addition one can observe an offset of the maximum of $A_{\theta_e}(\Phi_{max})$ to higher values of θ_e particularly for the Majorana ν_e s. Similar features can be observed in Fig. 6 for $\phi_v = \pi/4$.

It is necessary to point out that from the experimental point of view searches of differences between the Dirac and the Majorana ν_e s by the measurement of observables dependent on $(\hat{\eta}_v)^\perp$ would be extremely difficult. In order to measure $A_{\theta_e}(\Phi_{max})$ one should determine the location of Φ_{max} by counting the events from Φ to $\Phi + \pi$ and from $\Phi + \pi$ to $\Phi + 2\pi$ (for various Φ) at fixed θ_e (and a particular configuration of ϕ_v). In this way Φ_{max} and $A_{\theta_e}(\Phi_{max})$ are found according to their definitions. These measurements have to be repeated for different θ_e s. The experimental curve drawn with respect to θ_e should fit to one of the curves in Figs. 2, 5, 6. The measurement of $A(\Phi_{max})$ proceeds in a similar way, but now θ_e is not fixed - the azimuthal orientation of $(\hat{\eta}_v)^\perp$ described by ϕ_v is fixed instead. Events within the azimuthal angle from Φ to $\Phi + \pi$ and from $\Phi + \pi$ to $\Phi + 2\pi$ for all θ_e are counted. The repetitions of the measurements for different ϕ_v s give a curve which should fit to one of the curves in Fig. 4.

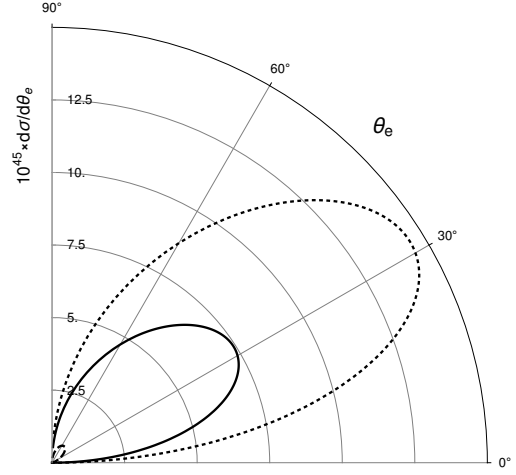


Fig. 7 Dirac (or Majorana) ν_e with $V - A$ interaction, $\hat{\eta}_v \cdot \hat{\mathbf{q}} = -1$, $E_v = 1 \text{ MeV}$: plot of $d\sigma/d\theta_e$ as a function of θ_e for different values of θ_1 ; dotted line for $\theta_1 = 0$; solid line for $\theta_1 = \pi/2$; dashed line for $\theta_1 = \pi$.

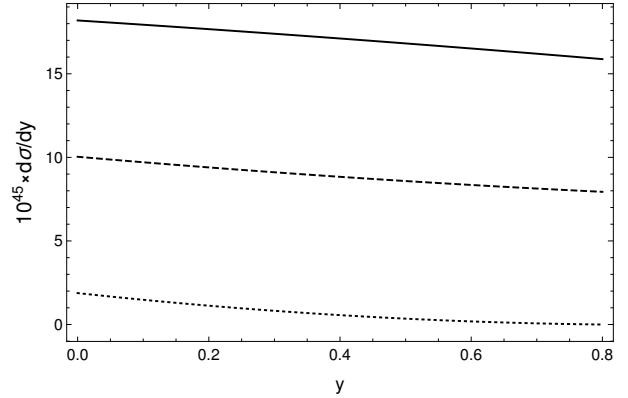


Fig. 8 Dirac (or Majorana) ν_e with $V - A$ interaction $\hat{\eta}_v \cdot \hat{\mathbf{q}} = -1$, $E_v = 1 \text{ MeV}$: plot of $d\sigma/dy$ as a function of y for different values of θ_1 : solid line for $\theta_1 = 0$; dashed line for $\theta_1 = \pi/2$; dotted line for $\theta_1 = \pi$.

5 Distinguishing between Dirac and Majorana neutrinos via spectrum and polar angle distribution of scattered electrons

In this section we explore the ν_e nature problem by using the electron energy spectrum and the polar angle distribution of scattered electrons. To begin with, it is worth recalling that the above observables do not allow one to differentiate between the Dirac and the Majorana ν_e s in the case of the standard $V - A$ interaction in the relativistic limit; see Figs. (7-8) plotted for $\theta_1 = 0, \pi/2, \pi$.

If one assumes that the ν_e source produces the superposition of LC with RC vs, the cross sections $d\sigma/d\theta_e$, $d\sigma/dy$ for the detection of Dirac and Majorana ν_e s contain the interferences between LC and RC vs proportional to the various angular correlations (T-even and T-odd) among $(\hat{\eta}_v)^\perp$, $\hat{\mathbf{q}}$, $\hat{\mathbf{p}}_e$, $(\hat{\eta}_e)^\perp$ vectors. Consequently the linear contributions

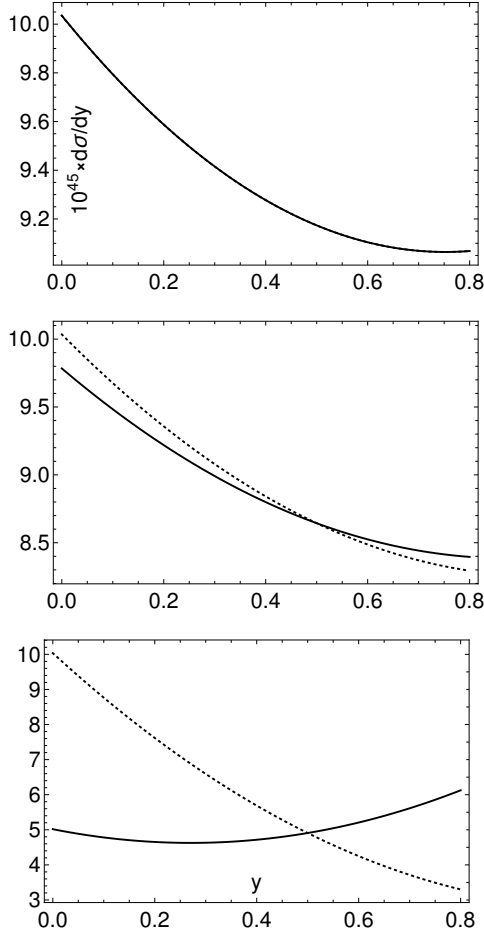


Fig. 9 $d\sigma/dy$ as a function of y for $V-A$ and S_R scenario with $c_S^R = 0.3$, $\theta_1 = \pi/2$; $\hat{\eta}_V \cdot \hat{\mathbf{q}} = -1$ (upper plot), $\hat{\eta}_V \cdot \hat{\mathbf{q}} = -0.95$ (middle plot), $\hat{\eta}_V \cdot \hat{\mathbf{q}} = 0$ (lower plot), for Dirac (solid line) and Majorana (dotted line) ν_e s.

from the non-standard interactions allow us to distinguish between the Dirac and the Majorana ν_e s, and search for TRSV, see Figs. (9-10).

Fig. 9 shows that it is possible to distinguish the neutrino nature in the case of $V-A$ and S interactions. Scalar couplings for both, the Dirac and the Majorana ν s, are constrained to give the same value of the spectrum at some specified value of y (in Fig. 9 $y = 0.5$ is fixed). It follows that the remaining freedom cannot be used to adjust the two cross sections. The diagrams in Fig.9 illustrate the generic behavior of spectra although they are plotted for a particular value of $|c_S^R| = 0.3$ defined for the Majorana ν_e (which, under the above constraint, determines a value of $|c_S^R|$ for the Dirac ν_e). The transversal polarization of the incoming ν_e plays here a crucial role, because only for $(\hat{\eta}_V)^\perp \neq 0$ one can discriminate between the Dirac and the Majorana neutrinos.

Fig. 10 shows how the change of θ_1 affects the energy spectrum of recoil electrons in the presence of interferences related to transversal component of the neutrino spin polariza-

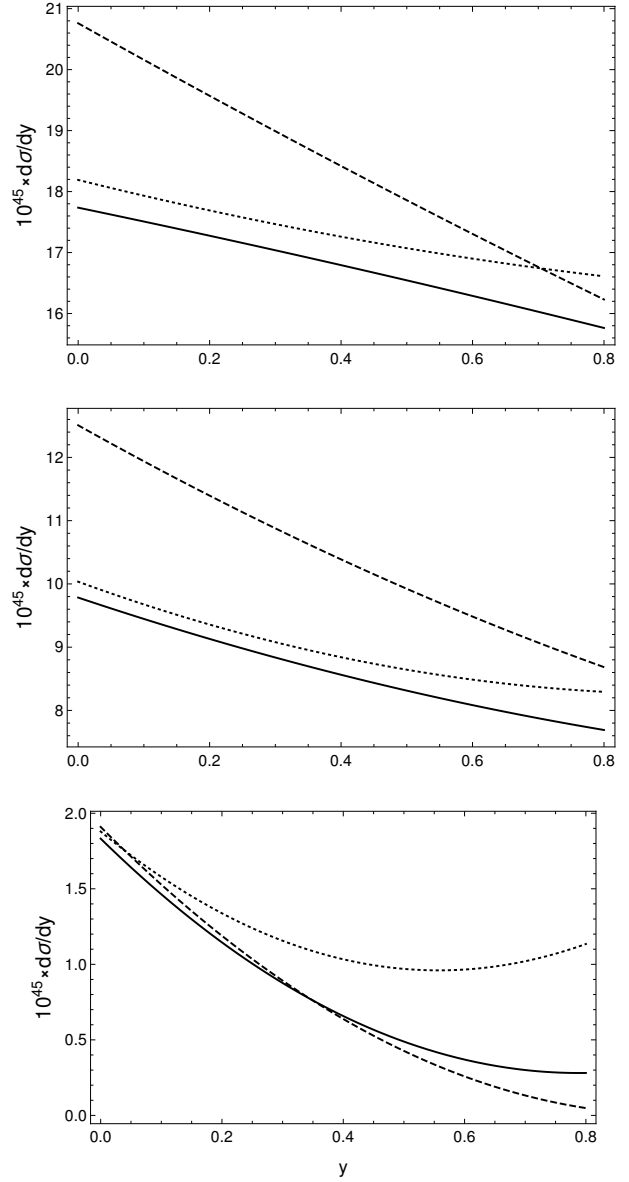


Fig. 10 Superposition of LC ν_e s with RC ones in presence of non-standard couplings with $\hat{\eta}_V \cdot \hat{\mathbf{q}} = -0.95$: dependence of $d\sigma/dy$ on y for different values of θ_1 when $E_V = 1 \text{ MeV}$, $\phi_V = 0$. Upper plot for $\theta_1 = 0$; middle plot for $\theta_1 = \pi/2$; lower plot for $\theta_1 = \pi$; dashed line for Dirac ν_e with $V-A$ and T_R , $|c_T^R| = 0.3$, $\theta_{T,R} = 0$; dotted line for Majorana ν_e with $V-A$ with S_R , $|c_S^R| = 0.3$, $\theta_{S,R} = 0$; solid line for Dirac ν_e with $V-A$ and S_R when $|c_S^R| = 0.3$, $\theta_{S,R} = 0$.

tion, both for the Dirac and the Majorana ν_e s; the plot should be compared with Fig.8. Small deviations for the low energy recoil electrons in the case of Dirac scenario with $V-A$ and T interactions when $\theta_1 = 0, \pi/2$ are seen (dashed line in upper and middle plots). On the other hand the departure from the standard prediction when $\theta_1 = \pi$ is too small to be clearly visible (lower plot). It is worth noting that Figs. (9-10) have been made at fixed azimuthal angle $\phi_V = 0$; changes of ϕ_V would affect the spectrum and polar distributions.

6 Conclusions

We have studied the two theoretically possible scenarios of the physics beyond the standard model in which flavour-conserving standard and non-standard interactions of both left chiral and right chiral electron neutrinos were introduced. We have shown that the various types of the azimuthal asymmetries of the recoil electrons, the energy spectrum and the polar angle distribution of the scattered electrons can in principle discern between the Dirac and the Majorana ν_e s interacting with PET both for the longitudinal and the transversal ν_e polarizations. The high-precision measurements of these quantities may shed some light on the fundamental problems of the ν nature and TRSV in the leptonic processes. In the particular case of the $V-A$ and S couplings the spectrum can distinguish the two types of the neutrinos as long as the incoming ν_e beam has non-vanishing transversal polarization. But even for the longitudinally polarized ν_e beam the asymmetry observable $A(\Phi)$ can identify the Dirac scenario with $V-A$, S and T interactions independently of any assumed Majorana non-standard couplings.

The proposed new tests require intensive monochromatic low-energy ν_e sources, large PET, and detectors enabling a measurement of the azimuthal angle and the polar angle of the recoil electrons with the high angular resolution. Propositions of the relevant detectors have been discussed in the literature [91–95]. In turn high-resolution measurements of the spectrum of low energy outgoing electrons demand detectors with the ultra low detection threshold and background noise. Some interesting concepts of various (monochromatic) ν_e sources are under debate [96–102]. A preliminary study of the feasibility of the electron polarized scintillating GSO target has been carried out by [40]. In order to make the detection of $(\hat{\eta}_\nu)^\perp$ -dependent effects possible, further studies on the appropriate choice of ν_e source which would take into account the exotic couplings of RC ν_e s are needed. This is necessary to explain the basic role of production processes in generating ν_e beam with non-zero transversal polarization and to control the azimuthal angle ϕ_ν . The controlled production of ν_e beam with the fixed direction of $(\hat{\eta}_\nu)^\perp$ with respect to the production plane is impossible to date, thus the alternative option with the (un)polarized ν_e source generating only the longitudinally polarized ν_e s seems to be presently more available.

7 Appendix 1 - General formula on laboratory differential cross section for elastic scattering of Majorana ν_e s on PET

The laboratory differential cross section for Majorana ν_e s, when $\hat{\eta}_e \perp \hat{\mathbf{q}}$ ($\theta_1 = \pi/2$), is of the form:

$$\frac{d^2\sigma}{dyd\phi_e} = \left(\frac{d^2\sigma}{dyd\phi_e} \right)_{V-A} + \left(\frac{d^2\sigma}{dyd\phi_e} \right)_{(S,P)_R} + \left(\frac{d^2\sigma}{dyd\phi_e} \right)_{V-A}^{S_R} + \left(\frac{d^2\sigma}{dyd\phi_e} \right)_{V-A}^{P_R} \quad (8)$$

$$\begin{aligned} \left(\frac{d^2\sigma}{dyd\phi_e} \right)_{V-A} = B \Bigg\{ & c_A^2 \left[(\hat{\eta}_e)^\perp \cdot (\hat{\mathbf{p}}_e)^\perp \hat{\eta}_\nu \cdot \hat{\mathbf{q}} (y-2) \right. \\ & \cdot \sqrt{y \left(\frac{2m_e}{E_\nu} + y \right) + y^2 - 2y + 2 + \frac{m_e}{E_\nu} y} \\ & + c_V^2 \left[(\hat{\eta}_e)^\perp \cdot (\hat{\mathbf{p}}_e)^\perp \hat{\eta}_\nu \cdot \hat{\mathbf{q}} y \sqrt{y \left(\frac{2m_e}{E_\nu} + y \right)} \right. \\ & \left. + y^2 - 2y + 2 - \frac{m_e}{E_\nu} y \right] \\ & + 2c_V c_A \left[(\hat{\eta}_e)^\perp \cdot (\hat{\mathbf{p}}_e)^\perp \sqrt{y \left(\frac{2m_e}{E_\nu} + y \right)} (y-1) \right. \\ & \left. + y(y-2) \hat{\eta}_\nu \cdot \hat{\mathbf{q}} \right] \Bigg\}, \end{aligned} \quad (9)$$

$$\begin{aligned} \left(\frac{d^2\sigma}{dyd\phi_e} \right)_{(S,P)_R} = B \Bigg\{ & y \left(y + 2 \frac{m_e}{E_\nu} \right) |c_S^R|^2 + y^2 |c_P^R|^2 \\ & - 4y \sqrt{y \left(\frac{2m_e}{E_\nu} + y \right)} (\hat{\eta}_e)^\perp \cdot (\hat{\mathbf{p}}_e)^\perp \hat{\eta}_\nu \cdot \hat{\mathbf{q}} \\ & \cdot [Re(c_S^R) Re(c_P^R) + Im(c_S^R) Im(c_P^R)] \Bigg\}, \end{aligned} \quad (10)$$

$$\begin{aligned} \left(\frac{d^2\sigma}{dyd\phi_e} \right)_{V-A}^{S_R} = 2B \Bigg\{ & 2c_V \sqrt{y \left(\frac{2m_e}{E_\nu} + y \right)} \\ & \cdot \left((\hat{\eta}_\nu)^\perp \cdot (\hat{\mathbf{q}} \times (\hat{\mathbf{p}}_e)^\perp) Im(c_S^R) + (\hat{\eta}_\nu)^\perp \cdot (\hat{\mathbf{p}}_e)^\perp Re(c_S^R) \right) \\ & - c_A \left(\frac{E_\nu}{m_e} y + 2 \right) \left[(\hat{\mathbf{p}}_e)^\perp \cdot ((\hat{\eta}_e)^\perp \times (\hat{\eta}_\nu)^\perp) Im(c_S^R) \right. \\ & \cdot \sqrt{y \left(\frac{2m_e}{E_\nu} + y \right) + y \left((\hat{\eta}_e)^\perp \cdot (\hat{\mathbf{p}}_e)^\perp \left((\hat{\eta}_\nu)^\perp \cdot (\hat{\mathbf{q}} \times (\hat{\mathbf{p}}_e)^\perp) \right. \right. \\ & \left. \left. \cdot Im(c_S^R) + (\hat{\eta}_\nu)^\perp \cdot (\hat{\mathbf{p}}_e)^\perp Re(c_S^R) \right) - Im(c_S^R) \right. \\ & \left. \left. \cdot \hat{\mathbf{q}} \cdot ((\hat{\eta}_e)^\perp \times (\hat{\eta}_\nu)^\perp) + \frac{m_e}{E_\nu} (\hat{\eta}_e)^\perp \cdot (\hat{\eta}_\nu)^\perp Re(c_S^R) \right) \right] \Bigg\}, \end{aligned} \quad (11)$$

$$\begin{aligned}
\left(\frac{d^2\sigma}{dyd\phi_e}\right)_{V-A}^{P_R} = & 2B c_A y \left\{ \frac{E_v}{m_e} y (\hat{\eta}_v)^\perp \cdot (\hat{\mathbf{p}}_e)^\perp \left(\text{Im}(c_P^R) \right. \right. \\
& \cdot (\hat{\eta}_e)^\perp \cdot (\hat{\mathbf{q}} \times (\hat{\mathbf{p}}_e)^\perp) + (\hat{\eta}_e)^\perp \cdot (\hat{\mathbf{p}}_e)^\perp \text{Re}(c_P^R) \Big) \\
& + 2(\hat{\eta}_v)^\perp \cdot (\hat{\mathbf{p}}_e)^\perp \left((\hat{\eta}_e)^\perp \cdot (\hat{\mathbf{q}} \times (\hat{\mathbf{p}}_e)^\perp) \text{Im}(c_P^R) + \text{Re}(c_P^R) \right. \\
& \cdot (\hat{\eta}_e)^\perp \cdot (\hat{\mathbf{p}}_e)^\perp \Big) + (y-2)(\hat{\eta}_e)^\perp \cdot (\hat{\eta}_v)^\perp \text{Re}(c_P^R) \\
& \left. - \sqrt{y \left(\frac{2m_e}{E_v} + y \right)} (\hat{\mathbf{p}}_e)^\perp \cdot ((\hat{\eta}_e)^\perp \times (\hat{\eta}_v)^\perp) \text{Im}(c_P^R) \right\},
\end{aligned} \quad (12)$$

where $B \equiv (E_v m_e / 2\pi^2) (G_F^2 / 2)$. $\hat{\eta}_v$ is the unit 3-vector of ν_e spin polarization in its rest frame, Fig. 1. $(\hat{\eta}_v \cdot \hat{\mathbf{q}})\hat{\mathbf{q}}$ is the longitudinal component of ν_e spin polarization. $|\hat{\eta}_v \cdot \hat{\mathbf{q}}| = |1 - 2Q_L^V|$, where Q_L^V is the probability of producing the LC ν_e . We see that the interference terms between standard $V - A$ and exotic S_R, P_R couplings depend on the transversal ν_e spin polarization $(\hat{\eta}_v)^\perp$ related to the production process (similar regularity as in the Dirac case [30]).

References

1. M. Doi et al., Phys. Lett. B **103**, 219 (1981)
2. W. C. Haxton et al., Phys. Rev. Lett. **47**, 153 (1981)
3. H. Ejiri, J. Phys. Soc. Jpn. **74**, 2101 (2005)
4. B. Kayser, R. E. Shrock, Phys. Lett. B **112**, 137 (1982)
5. P. Langacker, D. London, Phys. Rev. D **39**, 266 (1989)
6. S. L. Glashow, Nucl. Phys. **22**, 579 (1961)
7. S. Weinberg, Phys. Rev. Lett. **19**, 1264 (1967)
8. A. Salam, in *Elementary Particle Theory* (Almqvist and Wiksells, Stockholm, 1969)
9. R. P. Feynman, M. Gell-Mann, Phys. Rev. **109**, 193 (1958)
10. E. C. G. Sudarshan, R. E. Marshak, Phys. Rev. **109**, 1860 (1958)
11. S. P. Rosen, Phys. Rev. Lett. **48**, 842 (1982)
12. G. V. Dass, Phys. Rev. D **32**, 1239 (1985)
13. M. Zralek, Acta Phys. Polon. B **28**, 2225 (1997)
14. F. del Aguila, J. de Blas, R. Szafron, J. Wudka, M. Zralek, Phys. Lett. B **683**, 282 (2010)
15. M. Doi, T. Kotani, H. Nishiura, K. Okuda, E. Takasugi, Prog. Theor. Phys. **67**, 281 (1982)
16. V. B. Semikoz, Nucl. Phys. B **498**, 39 (1997)
17. S. Pastor, J. Segura, V. B. Semikoz, J. W. F. Valle, Phys. Rev. D **59**, 013004 (1998)
18. D. Singh, N. Mobed, G. Papini, Phys. Rev. Lett. **97**, 041101 (2006)
19. T. D. Gutierrez, Phys. Rev. Lett. **96**, 121802 (2006)
20. W. Rodejohann, Xun-Jie Xu, C. E. Yaguna, JHEP **05**, 024 (2017)
21. Xun-Jie Xu, Phys. Rev. D **99**, 075003 (2019)
22. A. de Gouvea, J. Jenkins, Phys. Rev. D **74**, 033004 (2006)
23. M. Carena, A. de Gouvea, A. Freitas, M. Schmitt, Phys. Rev. D **68**, 113007 (2003)
24. P. Stockinger, W. Grimus, Phys. Lett. B **327**, 327 (1994)
25. M. Misiasek et al., Nucl. Phys. B **734**, 203 (2006)
26. P. Minkowski, M. Passera, Phys. Lett. B **541**, 151 (2002)
27. T. I. Rashba, V. B. Semikoz, Phys. Lett. B **479**, 218 (2000)
28. J. Bernabeu et al., Phys. Lett. B **613**, 162 (2005)
29. S. Ciechanowicz et al., Phys. Rev. D **71**, 093006 (2005)
30. W. Sobk6w, A. Błaut, Eur. Phys. J. C **78**, 197 (2018)
31. V. A. Guseinov et al., Phys. Rev. D **75**, 073021 (2007)
32. W.-T. Ni et al., Phys. Rev. Lett. **82**, 2439 (1999)
33. W. Bialek et al., Phys. Rev. Lett. **56**, 1623 (1986)
34. P. V. Vorobyov, Y. I. Gitarts, Phys. Lett. B **208**, 146 (1988)
35. C.-T. Chiang, M. Kamionkowski, G. Z. Krnjaic, Phys. Dark Univ. **1**, 109 (2012)
36. T. Franarin, M. Fairbairn, Phys. Rev. D **94**, 053004, (2016)
37. G. D. Starkman, D. N. Spergel, Phys. Rev. Lett. **74**, 2623 (1995)
38. M. A. Bouchiat, T. R. Carver, C. M. Varnum, Phys. Rev. Lett. **5**, 373 (1960)
39. T. G. Walker, W. Happer, Rev. Mod. Phys. **69**, 629 (1997)
40. B. Babussinov et al., Nucl. Instrum. and Meth. A **694**, 335 (2012)
41. A. Riotto, M. Trodden, Annu. Rev. Nucl. Part. Sci. **49**, 35 (1999)
42. M. Kobayashi, T. Maskawa, Prog. Theor. Phys. **49**, 652 (1973)
43. J.C. Pati, A. Salam, Phys. Rev. D **10**, 275 (1974)
44. R. Mohapatra, J.C. Pati, Phys. Rev. D **11**, 566 (1975); Phys. Rev. D **11**, 558 (1975)
45. R.N. Mohapatra, G. Senjanovic, Phys. Rev. D **12**, 1502 (1975)
46. M. A. B. Beg et al., Phys. Rev. Lett. **38**, 1252 (1977)
47. A. Jodidio et al., Phys. Rev. D **34**, 1967 (1986)
48. E. J. Eichten, K. D. Lane, M.E. Peskin, Phys. Rev. Lett. **50**, 811 (1983)
49. P. Herczeg, Prog. Part. Nucl. Phys. **46**, 413 (2001)
50. N. Arkani-Hamed, S. Dimopoulos, G. Dvali, J. March-Russell, Phys. Lett. B **429**, 263 (1998)
51. T. Banks, A. Zaks, Nucl. Phys. B **196**, 189 (1982)
52. H. Georgi, Phys. Rev. Lett. **98**, 221601 (2007)
53. H. Georgi, Phys. Lett. B **650**, 275 (2007)
54. K. Cheung, W.Y. Keung, T.C. Yuan, Phys. Rev. Lett. **99**, 051803 (2007)
55. S. L. Chen, X. G. He, Phys. Rev. D **76**, 091702 (2007)

56. A. B. Balantekin, K. O. Ozansoy, Phys. Rev. D **76**, 095014 (2007)
57. J. Barranco et al., Phys. Rev. D **79**, 073011 (2009)
58. D. Montanino, M. Picariello, J. Pulido, Phys. Rev. D **77**, 093011 (2008)
59. S. Zhou, Phys. Lett. B **659**, 336 (2008)
60. B. Grinstein, K. A. Intriligator, I. Z. Rothstein, Phys. Lett. B **662**, 367 (2008)
61. J. Barranco et al., Int. J. Mod. Phys. A **27**, 1250147 (2012)
62. L. Wolfenstein, Phys. Rev. D **17**, 2369 (1978)
63. J. W. F. Valle, Phys. Lett. B **199**, 432 (1987)
64. E. Roulet, Phys. Rev. D **44**, 935 (1991)
65. M. M. Guzzo, A. Masiero, S. T. Petcov, Phys. Lett. B **260**, 154 (1991)
66. J. Schechter, J. W. F. Valle, Phys. Rev. D **22**, 2227 (1980)
67. A. Zee, Phys. Lett. B **93**, 389 (1980)
68. L. J. Hall, V. A. Kostelecky, S. Raby, Nucl. Phys. B **267**, 415 (1986)
69. K. S. Babu, Phys. Lett. B **203**, 132 (1988)
70. M. Hirsch, J. W. F. Valle, New J. Phys. **6**, 76 (2004)
71. N. Fornengo et al., Phys. Rev. D **65**, 013010 (2001)
72. P. S. Amanik, G. M. Fuller, B. Grinstein, Astropart. Phys. **24**, 160 (2005)
73. O. G. Miranda, M. Maya, R. Huerta, Phys. Rev. D **53**, 1719 (1996)
74. O. G. Miranda, V. Semikoz, J. W. F. Valle, Nucl. Phys. Proc. Suppl. **66**, 261 (1998)
75. J. Barranco, O. G. Miranda, T. I. Rashba, Phys. Rev. D **76**, 073008 (2007)
76. A. Bolanos et al., Phys. Rev. D **79**, 113012 (2009)
77. S. Davidson et al., JHEP **0303**, 011 (2003)
78. Z. Berezhiani, R.S. Raghavan, A. Rossi, Nucl. Phys. B **638**, 62 (2002)
79. J. Barranco et al., Phys. Rev. D **77**, 093014 (2008)
80. C. Biggio, M. Blennow, E. Fernandez-Martinez, JHEP **0903**, 139 (2009)
81. K. Scholberg, Phys. Rev. D **73**, 033005 (2006)
82. J. Barranco et al., Phys. Lett. B **739**, 343 (2014)
83. J. Barranco et al., J. Phys. G: Nucl. Part. Phys. **47**, 035201 (2020)
84. M. Tanabashi et al. (Particle Data Group), Phys. Rev. D **98**, 030001 (2018)
85. S. Sobk  w, A. B  aut, Eur. Phys. J. C **76**, 550 (2016)
86. M. Deniz et al., Phys. Rev. D **82**, 033004 (2010)
87. M. Deniz et al., Phys. Rev. D **95**, 033008 (2017)
88. L. Michel, A. S. Wightman, Phys. Rev. **98**, 1190 (1955)
89. S. Ciechanowicz, M. Misiaszek, S. Sobk  w, Eur. Phys. J. C **32**, s01, s151 (2003)
90. D. M. Webber et al., Phys. Rev. Lett. **106**, 041803 (2011)
91. F. Arzarello et al., Report No. CERN-LAA/94-19, College de France LPC/94-28, 1994
92. J. Seguinot et al., Report No. LPC 95 08, College de France, Laboratoire de Physique Corpusculaire, 1995
93. A. Sarrat, Nucl. Phys. Proc. Suppl. **95**, 177 (2001)
94. R. E. Lanou et al., The Heron project, Abstracts of Papers of the American Chemical Society 2(217), 021-NUCL 1999
95. Y.H. Huang, R. E. Lanou, H. J. Maris, G. M. Seidel, B. Sethumadhavan, W. Yao, Astropart. Phys. **30**, 1 (2008)
96. P. Zucchelli, Phys. Lett. B **532**, 166 (2002)
97. J. Sato, Phys. Rev. Lett. **95**, 131804 (2005)
98. J. Bernabeu, J. Burguet-Castell, C. Espinoza, M. Lindroos, JHEP, issue **12**, 14 (2005)
99. A. L. Barabanov, O. A. Titov, Eur. Phys. J. A **51**, 96 (2015)
100. A. L. Barabanov, O. A. Titov, Phys. Rev. C **99**, 045502 (2019)
101. J. Bernabeu, C. Espinoza, C. Orme, S. Palomares-Ruiz, S. Pascoli, JHEP, issue **06**, 040 (2009)
102. M. E. Estevez Aguado et al., Phys. Rev. C **84**, 034304 (2011)